Unidirectional Eph/ephrin signaling creates a cortical actomyosin differential to drive cell segregation

Audrey K. O'Neill,[1] Abigail A. Kindberg,[1,2]* Terren K. Niethamer,[1,2]* Andrew R. Larson,[1] Hsin-Yi Henry Ho,[4,5] Michael E. Greenberg,[5] and Jeffrey O. Bush[1,2,3]

[1]Department of Cell and Tissue Biology, Program in Craniofacial Biology and Institute for Human Genetics, [2]Biomedical Sciences Graduate Program, and [3]Eli and Edythe Broad Center of Regeneration Medicine and Stem Cell Research, University of California, San Francisco, San Francisco, CA 94143
[4]Department of Cell Biology and Human Anatomy, University of California Davis School of Medicine, Davis, CA 95817
[5]Department of Neurobiology, Harvard Medical School, Boston, MA 02115

Cell segregation is the process by which cells self-organize to establish developmental boundaries, an essential step in tissue formation. Cell segregation is a common outcome of Eph/ephrin signaling, but the mechanisms remain unclear. In craniofrontonasal syndrome, X-linked mosaicism for ephrin-B1 expression has been hypothesized to lead to aberrant Eph/ephrin-mediated cell segregation. Here, we use mouse genetics to exploit mosaicism to study cell segregation in the mammalian embryo and integrate live-cell imaging to examine the underlying cellular and molecular mechanisms. Our data demonstrate that dramatic ephrin-B1–mediated cell segregation occurs in the early neuroepithelium. In contrast to the paradigm that repulsive bidirectional signaling drives cell segregation, unidirectional EphB kinase signaling leads to cell sorting by the Rho kinase–dependent generation of a cortical actin differential between ephrin-B1– and EphB-expressing cells. These results define mechanisms of Eph/ephrin-mediated cell segregation, implicating unidirectional regulation of cortical actomyosin contractility as a key effector of this fundamental process.

Introduction

Normal development requires the self-organization of cells by sorting or segregation to establish and maintain boundaries and ultimately form distinct tissues in the adult organism (Fagotto, 2014). Cellular segregation can be achieved by three general cellular mechanisms, namely differential adhesion, cell–cell repulsion, and differential interfacial tension (Batlle and Wilkinson, 2012; Fagotto et al., 2014; Cayuso et al., 2015). The differential adhesion hypothesis proposes that differences in adhesion between cell populations driven by qualitative or quantitative differences in the expression of cell adhesion molecules will drive the more adhesive population to segregate to the inside of the less adhesive population (Steinberg, 1963, 1970; Batlle and Wilkinson, 2012). Models of segregation involving cell–cell repulsion predict that segregating cells are repelled by and migrate directionally away from one another, eventually resulting in segregation. In contrast, the differential interfacial tension hypothesis (DITH) proposes that segregation is caused by differences in cortical tension between cells leading to a change in the force of the cell–cell contact, or interfacial tension. The actomyosin cytoskeleton is thought to be critical for interfacial tension–driven segregation, with prominent F-actin cables often forming at heterotypic boundaries, and cells with

differences in Rho kinase (ROCK) activity segregate in vitro (Krieg et al., 2008; Monier et al., 2010).

The Eph/ephrin family of signaling molecules mediates boundary formation during many developmental processes across organisms, including the development of rhombomeres, the eye, limb buds, somites, cranial sutures, and intestinal crypts in vertebrates, as well as in *Drosophila melanogaster* wing discs (Durbin et al., 1998; Xu et al., 1999; Santiago and Erickson, 2002; Barrios et al., 2003; Wada et al., 2003; Holmberg et al., 2006; Merrill et al., 2006; Ting et al., 2009; Cavodeassi et al., 2013; Umetsu et al., 2014). B-type ephrins are transmembrane proteins that bind to EphB receptors on neighboring cells and can signal bidirectionally. They stimulate "forward" signaling by activation of EphB receptor signaling and "reverse" signaling through SH2 and PDZ (named for PSD95, Dlg1, and ZO-1) adaptor proteins that bind to conserved phosphorylated tyrosines and PDZ ligands, respectively, on the intracellular domain of B-type ephrins. Forward signaling has been proposed to occur via both kinase-dependent and kinase-independent mechanisms (Birgbauer et al., 2000; Holmberg et al., 2006; Dravis and Henkemeyer, 2011). Numerous cell culture and explant studies have investigated Eph/ephrin downstream signaling pathways, revealing important roles for Rho family GTPase signaling, though no

Streak stage (E7.75)   Headfold stage (E8.0)   Somite stage (E8.5)

$Efnb1^{+XGFP/lox}$ $Efnb1^{+XGFP/\Delta}$ $Efnb1^{+XGFP/lox}$ $Efnb1^{+XGFP/\Delta}$ $Efnb1^{+XGFP/lox}$ $Efnb1^{+XGFP/\Delta}$
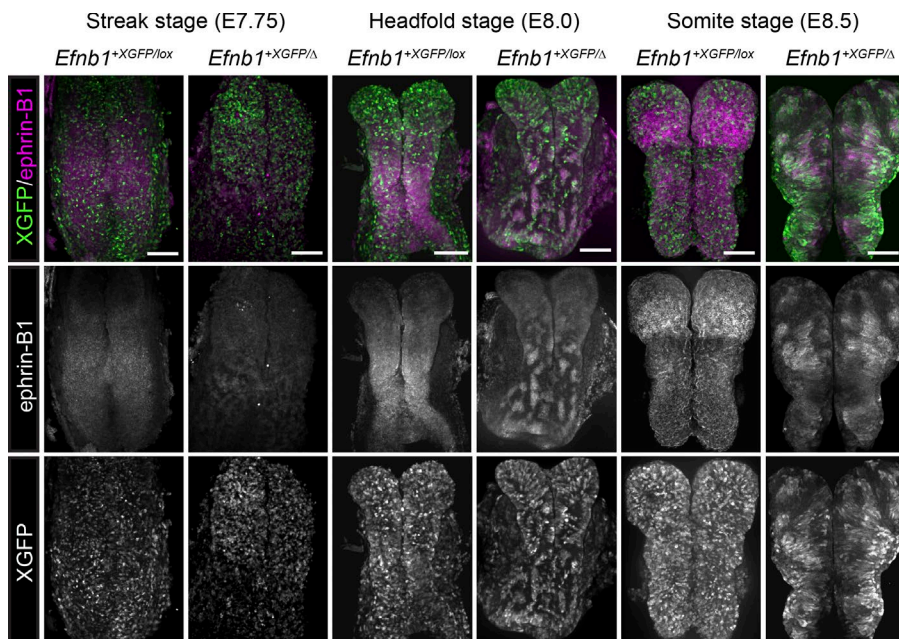
XGFP/ephrin-B1

ephrin-B1

XGFP

Figure 1. **Ephrin-B1–mediated cell segregation in mice occurs in the neuroepithelium at E8.5.** Comparison of $Efnb1^{+XGFP/\Delta}$ heterozygote and control ($Efnb1^{+XGFP/lox}$) mouse embryos stained for ephrin-B1 (magenta) and GFP (green) at E7.75–E8.5. Numbers of embryos analyzed are presented in Table S2. Bars, 150 µm. See also Fig. S1.

genetic studies in intact embryos have yet been reported (Tanaka et al., 2003; Rohani et al., 2011; Nievergall et al., 2012). The current paradigm, derived mostly from overexpression studies, proposes that bidirectional Eph/ephrin signaling mediates changes in adhesion and repulsive migration to drive cell segregation; whether differential interfacial tension contributes to Eph/ephrin cell segregation is unknown (Xu et al., 1999; Poliakov et al., 2008; Jørgensen et al., 2009; Rohani et al., 2011; Prospéri et al., 2015).

To study the mechanisms underlying Eph/ephrin-mediated cell segregation, we use a genetic mouse model involving mosaicism for ephrin-B1. This model arose out of interest in the human disease craniofrontonasal syndrome (CFNS; MIM304110). CFNS results from mutation of the X-linked gene *EFNB1*, which encodes EPHRINB1, and is unusual in that heterozygous females display severe phenotypes, whereas hemizygous males are only mildly affected (Twigg et al., 2004; Wieland et al., 2004). Mosaicism for ephrin-B1 function appears to be central to disease severity, because male patients with somatic, as opposed to germline, mutations in *EFNB1* exhibit severe manifestations of CFNS (Twigg et al., 2013). This aspect of the disease is phenocopied in $Efnb1^{\Delta/+}$ mice, which display more severe dysmorphogenesis than either hemizygous-null ($Efnb1^{\Delta/Y}$) males or homozygous-null ($Efnb1^{\Delta/\Delta}$) females (Compagni et al., 2003; Davy et al., 2004, 2006; Bush and Soriano, 2010). In $Efnb1^{\Delta/+}$ embryos, random X-inactivation, which occurs at around embryonic day 5.5 (E5.5), results in the silencing of either the mutant or the wild-type (WT) allele, thereby generating mosaicism in which half of the cells are capable of expressing WT ephrin-B1 (from the unaffected X chromosome) and half of the cells cannot express a functional copy of ephrin-B1. These populations have been reported to appear as large patches in the limb bud and secondary palate, with the formation of aberrant boundaries between ephrin-B1–expressing and nonexpressing regions that often correlate with regions of dysmorphogenesis (Compagni et al., 2003; Davy et al., 2006; Bush and Soriano, 2010). That *Efnb1* is X linked thus provides a unique opportunity to study cellular segregation in the mammalian

embryo; in this system, dramatic, developmentally important segregation results from mosaicism for the expression of only one molecule. By combining mouse genetics and live imaging studies, we examine the molecular and cellular drivers of this cell segregation and propose a novel model, based on cortical tension, for how it occurs.

Results

Ephrin-B1–driven cell segregation in mice

To visualize cell segregation in $Efnb1^{\Delta/+}$ mouse embryos, we used an X-linked β-actin–GFP transgene (XGFP) that results in a fine-grained mosaic pattern of GFP expression in females heterozygous for this transgene caused by random X-inactivation (Hadjantonakis et al., 1998, 2001; Compagni et al., 2003). To determine the onset of cell segregation, we examined $Efnb1^{+XGFP/\Delta}$ embryos at progressive stages of development by immunostaining for ephrin-B1 and GFP. At the late streak stage (E7.75), we observed an apparently random, evenly distributed and fine-grained pattern of mosaic GFP expression throughout $Efnb1^{+XGFP/\Delta}$ embryos that was indistinguishable from that observed in $Efnb1^{+XGFP/lox}$ controls (Fig. 1, left columns). At the early headfold stage (E8.0; zero to two somites), coincident with the appearance of ephrin-B1 expression (Fig. 1 and Fig. S1), we began to observe the establishment of ephrin-B1–positive, GFP-positive patches that were absent in controls (Fig. 1, center columns). By E8.5 (five to eight somites), around the initiation of neural crest cell emigration, $Efnb1^{+XGFP/\Delta}$ embryos exhibited robust ephrin-B1–driven segregation in the neuroepithelium (Fig. 1, right columns). Thus, ephrin-B1–driven cell segregation occurs in the neuroepithelium progenitor population shortly after the onset of ephrin-B1 expression. We therefore focused on the neuroepithelium to examine mechanisms of Eph/ephrin cell segregation.

Unidirectional signaling drives segregation

Previous studies have indicated that bidirectional signaling drives cell segregation (Xu et al., 1999; Mellitzer et al., 2000;
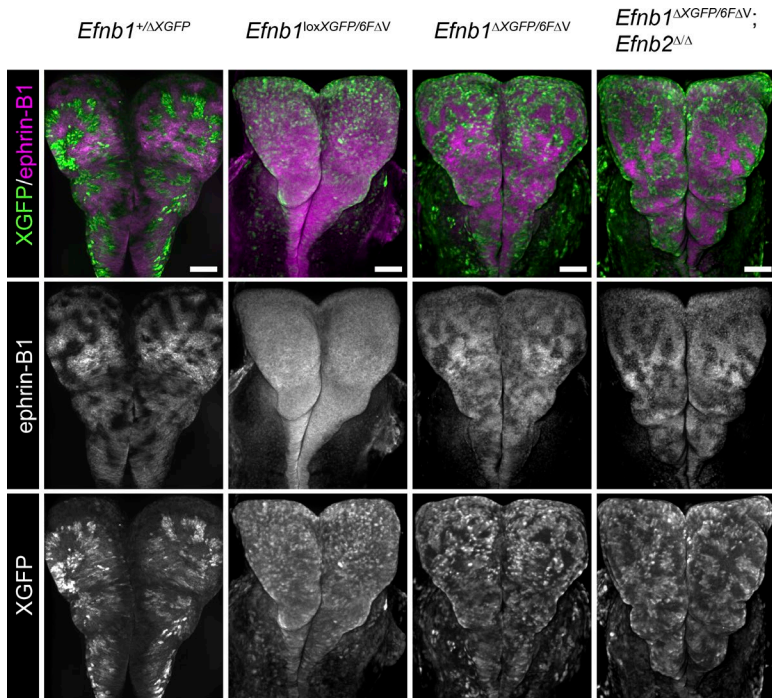
$Efnb1^{+/\Delta XGFP}$ $Efnb1^{loxXGFP/6F\Delta V}$ $Efnb1^{\Delta XGFP/6F\Delta V}$ $Efnb1^{\Delta XGFP/6F\Delta V};$ $Efnb2^{\Delta/\Delta}$

XGFP/ephrin-B1

ephrin-B1

XGFP

Figure 2. **Reverse signaling is dispensable for cell segregation in $Efnb1^{\Delta/+}$ neuroepithelium.** E8.5 mouse embryos expressing various combinations of $Efnb$ alleles. 6FΔV, reverse signaling dead allele. Numbers of embryos analyzed are presented in Table S2. The GFP signal was adjusted in a nonlinear fashion to assist discrimination of the ephrin-B1–negative population. Bars, 100 µm.

Jørgensen et al., 2009). To determine whether ephrin-B1 drives segregation through forward and/or reverse signaling in the neuroepithelium, we used several mutant alleles to selectively ablate specific downstream signaling cascades in the context of $Efnb1$ heterozygosity. These experiments required that the X-linked GFP and mutated $Efnb1$ allele be located on the same X chromosome, so we selected for recombination between these unlinked loci and obtained $Efnb1^{+/\Delta XGFP}$ embryos that express XGFP in ephrin-B1–null cells (Fig. 2, first column). We first tested the involvement of reverse signaling using the $Efnb1^{6F\Delta V}$ allele, which lacks reverse signaling through known mechanisms because of mutations of the six phosphorylatable intracellular tyrosines and deletion of the C-terminal valine, which is required for binding PDZ domain proteins (Bush and Soriano, 2009). We reasoned that $Efnb1^{loxXGFP/6F\Delta V}$ embryos, in which half of the cells lack the ability to receive a reverse signal and half express WT ephrin-B1, should exhibit cell segregation only if mosaic loss of reverse signaling is sufficient for this process. However, contrary to this prediction, the XGFP distribution in E8.5 embryos showed no cell segregation but instead exhibited a uniform and fine-grained mosaic distribution of GFP-positive cells (Fig. 2, second column). To determine whether phosphotyrosine- or PDZ-dependent reverse signaling is required for cell sorting, we generated $Efnb1^{\Delta XGFP/6F\Delta V}$ embryos, in which half of the cells are incapable of reverse signaling and the other half have no ephrin-B1 at all. These embryos exhibited dramatic cell segregation that was indistinguishable from that seen in $Efnb1^{+/\Delta XGFP}$ embryos, indicating that completely eliminating phosphotyrosine- and PDZ-dependent reverse signaling in the context of ephrin-B1 mosaicism did not diminish cell segregation (Fig. 2, third column). Furthermore, this was not attributable to functional compensation for ephrin-B1 reverse signaling by the closely related family member ephrin-B2, because $Efnb1^{\Delta XGFP/6F\Delta V};Efnb2^{\Delta/\Delta}$ embryos also exhibited cell segregation comparable to that seen in $Efnb1^{+/\Delta XGFP}$ embryos (Fig. 2, last column). Therefore, reverse signaling through these mechanisms is not sufficient or necessary for ephrin-B1–driven cell segregation.

If cell segregation is indeed driven exclusively by activating forward signaling, then withdrawal of forward signal transduction in the context of ephrin-B1 mosaicism should block the ability of cells to segregate. EphB2 and EphB3 have been shown to have redundant roles as receptors for ephrin-B1 (Orioli et al., 1996; Risley et al., 2009), and both are expressed in the neuroepithelium at E8.5 (Fig. S1). Deletion of one or both copies of $Ephb3$ in $Efnb1^{+/\Delta XGFP}$ mutant embryos did not have a notable effect on cell segregation (Fig. 3, first and second columns). However, removing EphB2 forward signaling using an allele in which the cytosolic domain is replaced with LacZ ($Ephb2^{LacZ}$; Orioli et al., 1996) resulted in a striking reduction of cell segregation in $Efnb1^{+/\Delta XGFP};Ephb2^{LacZ/LacZ}$ embryos, and compound loss of EphB2 forward signaling and EphB3 (in $Efnb1^{+/\Delta XGFP};Ephb2^{LacZ/LacZ};Ephb3^{-/-}$ embryos) completely abrogated cell segregation (Fig. 3, third and fourth columns). Contrary to the prevailing model of bidirectional Eph/ephrin-driven segregation, our results demonstrate that forward signaling alone drives cell segregation.

Because kinase-dependent and -independent modes of forward signaling have been described (Dravis and Henkemeyer, 2011), we asked which of these are required for ephrin-B1–mediated cell segregation. To address this, we used a chemical genetics approach involving mutant knock-in alleles of the EphB1, EphB2, and EphB3 kinases in which the ATP binding pockets were engineered to be inhibited by bulky analogs of the Src inhibitor PP1 ($Ephb1^{AS-KI}$, $Ephb2^{AS-KI}$, and $Ephb3^{AS-KI}$; Soskis et al., 2012). This approach enables the specific and reversible inhibition of EphB receptors at various times during development by treatment with 1-NA-PP1. We treated $Efnb1^{+/\Delta XGFP}$ embryos expressing either WT ($Ephb^{+/+}$) or analog-sensitive ($Ephb^{AS-TKI/AS-TKI}$) EphB1, EphB2, and EphB3 with 1-NA-PP1 or vehicle every 8 h from E7.5 to E8.5 and examined the effect on cell segregation. Segregation was dramatically reduced in $Efnb1^{+/\Delta XGFP};Ephb^{AS-TKI/AS-TKI}$ embryos treated with 1-NA-PP1 (Fig. 4, third column) compared with controls, indicating that kinase-dependent signaling through
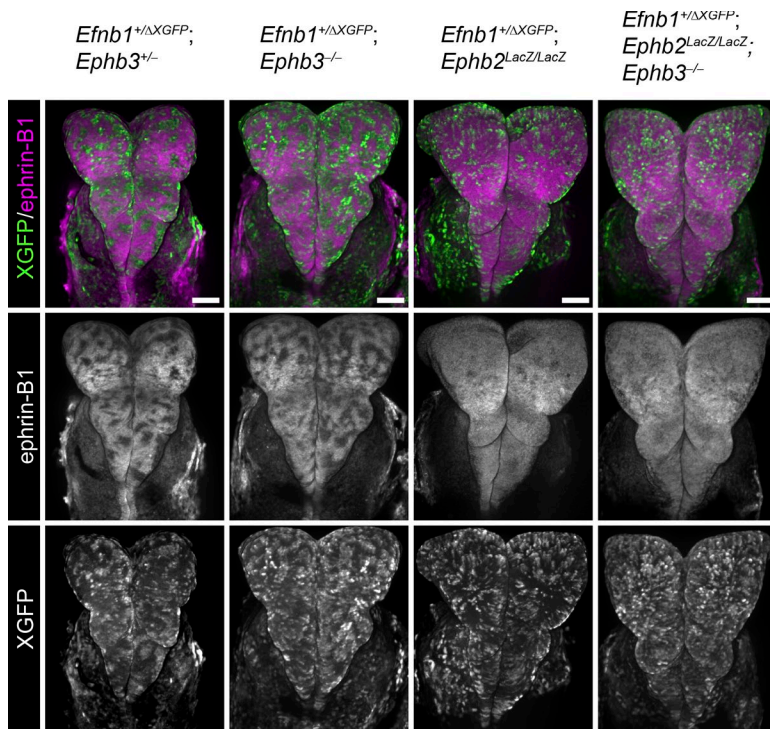
Figure 3. **Forward signaling is critical for cell segregation in *Efnb1*^Δ/+ neuroepithelium.** E8.5 *Efnb1*^ΔXGFP/+ mouse embryos with various combinations of Eph receptor mutations. LacZ, forward signaling dead allele. Numbers of embryos analyzed are presented in Table S2. The GFP signal was adjusted in a nonlinear fashion to assist discrimination of the ephrin-B1–negative population. Bars, 100 µm.

EphB receptors is crucial for ephrin-B1–mediated cell segregation in the neuroepithelium. Collectively, these results demonstrate that kinase-dependent forward signaling is critical for ephrin-B1–mediated cell sorting.

Forward signaling generates a cortical actin differential during segregation

To determine how unidirectional signaling could mediate cell segregation behaviors, we turned to a HEK293 model in which ephrin-B1 and EphB2 are expressed in two separate populations of cells (with the EphB2 population marked with GFP; Poliakov et al., 2008). After mixing of these two populations, the cells undergo segregation into large EphB2-expressing domains surrounded by ephrin-B1–expressing cells (see Fig. S4 and Materials and methods for more details; Poliakov et al., 2008). Live imaging of segregation revealed that the EphB2 cells underwent repeated rounds of collapse and cell rounding upon contact with ephrin-B1 cells, as previously observed (Video 1).
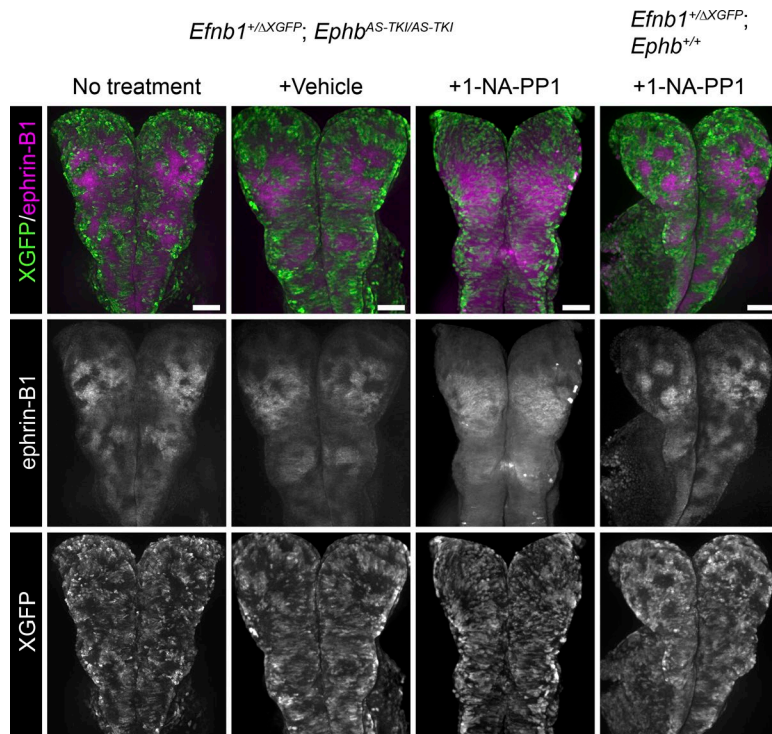

Figure 4. **Cell segregation relies on kinase-dependent signaling through EphB receptors.** E8.5 *Efnb1*^ΔXGFP/+ mouse embryos with analog-sensitive kinase mutations in EphB1, EphB2, and EphB3 (*Ephb*^AS-TKI/AS-TKI) or WT EphBs (*Ephb*^+/+), treated with vehicle or 1-NA-PP1. Numbers of embryos analyzed are presented in Table S2. The GFP signal was adjusted in a nonlinear fashion to assist discrimination of the ephrin-B1–negative population. Bars, 100 µm.

One current paradigm suggests that cell sorting is driven by repulsive migration of segregating cells away from each other over repeated interactions (Poliakov et al., 2004, 2008; Taylor et al., 2012). We therefore asked if repeated unidirectional repulsion of EphB2 cells, driven by forward signaling from ephrin-B1 cells, progressively redirected EphB2 cells into larger clusters. We reasoned that if repeated repulsive migration and redirection drives cell segregation, we would expect an increase in the overall distance EphB2 cells travel when cultured with ephrin-B1 cells when compared with EphB2 cells cultured with other EphB2 cells. Indeed, at low cell densities at which cells could move freely but segregation was not observed, we were able to detect an increase in the migratory distance of EphB2 cells when in co-culture with ephrin-B1 cells (Fig. S3 C), consistent with the documented capacity of Eph/ephrin-B1 signaling to regulate repulsive migration (Poliakov et al., 2008). On the contrary, when we tracked EphB2 cells over 16 h of live imaging under higher-density conditions in which cell segregation was observed, we found that EphB2 cell overall movement was actually slightly decreased when in co-culture with ephrin-B1 cells (Fig. 5 C), showing that repulsive migration was not likely to solely drive cell segregation.

We therefore asked whether another model of segregation, the DITH, might better explain Eph/ephrin-mediated cell sorting. The DITH states that differences in cortical tension between two populations of cells lead to differences in their interfacial tension and can drive cell segregation. To examine changes in cortical tension and the actin cytoskeleton in this system, we stably expressed the fluorescent F-actin reporter LifeAct-mCherry (Riedl et al., 2008) in both cell types and used time-lapse confocal microscopy to examine the cells for 16 h starting 1 h after mixing. We noted a dramatic increase in the intensity of LifeAct-mCherry fluorescence in the EphB2 population (Fig. 5 A, white arrowheads), but not the ephrin-B1 population (Fig. 5 A, yellow arrowheads), upon contact between the two cell types as cell sorting proceeded (Video 1; Fig. 5, A and B, top rows; and Fig. 5, D, E, G, and H). Although LifeAct-mCherry fluorescence intensity increased throughout the EphB2 cells (Fig. 5, A and B), the increase was most dramatic at the cell cortex (Fig. 5, compare D and E). This increase was present at early time points, suggesting that increased cortical actin is not simply a consequence of sorting (Fig. 5, D and E). Furthermore, as sorting proceeded, EphB2-expressing cells coalesced into tight groups, with pronounced elevation of cortical actin at the outer borders of EphB2-positive cell groups (Fig. 5 F). LifeAct fluorescence also increased in EphB2 cells interacting with ephrin-B1 cells at low cell density, indicating that the increase was not caused by the cells being constrained or by increasing overlap of EphB2 membranes (Videos 5 and 6; and Fig. S3, D and E). An increase in cortical actin was not observed in control conditions in which EphB2 cells were mixed with themselves or when ephrin-B1 cells were mixed with untransfected 293 cells (Videos 3 and 4; Fig. 5, D–H; and Fig. S2, A and B). Therefore, consistent with our genetic data pointing to unidirectional signaling as the driver of cell sorting, forward signaling results in an increase in cortical actin in only the EphB2 population, leading to a differential between the two cell populations.

We next determined the involvement of signaling pathways downstream of Eph receptors in this process. Eph signaling is complex and involves multiple effectors, including Rho and Ras family GTPases, the phosphoinositide 3-kinase (PI3K)–

Akt pathway, p21-activated kinases, focal adhesion kinases and E-cadherin cleavage via the protease ADAM10 (Poliakov et al., 2008; Shi et al., 2009; Bush and Soriano, 2010; Solanas et al., 2011; Nievergall et al., 2012; Lisabeth et al., 2013; Choe and Crump, 2015). Given the number of potential mechanisms involved, we performed pharmacological screening of candidate mediator pathways to determine which might have dominant involvement (Fig. S4; see Materials and methods section for further description; Poliakov et al., 2008). Upon treatment of mixed cell populations, we performed nearest-neighbor analysis to compare the extent of segregation upon treatment with different inhibitors. We observed slight but nonsignificant decreases in sorting with many of the inhibitors, consistent with the known roles of their targets in EphB signaling. Surprisingly, the MEK inhibitor U0126 did not significantly affect sorting, and the PI3K inhibitor GDC0941 significantly increased segregation. Of the inhibitors we tested, we observed statistically significant reduction of cell segregation only upon treatment with inhibitors of ROCK or myosin light chain kinase. Based on these findings, we examined the effect of inhibiting ROCK activity on cortical actomyosin accumulation by live imaging. At the beginning of cell mixing, the LifeAct-mCherry fluorescence intensity in EphB2 cells treated with ROCK inhibitor (Y-27632) was comparable to control; although cortical actin increased dramatically in control cells as sorting proceeded, it did not upon inhibition of ROCK activity (Video 2 and Fig. 5, A and B [bottom] and D–F). To confirm the specificity of Y-27632 and to determine whether ROCK function was specifically required in EphB2 cells, we used CRISPR/Cas9 mutagenesis to knock out ROCK1 and ROCK2 in EphB2-expressing cells and examined F-actin during segregation using phalloidin staining. We found that genetic ablation of ROCK function decreased cortical actin intensity, similar to treatment with Y-27632 (Fig. S5). Thus, we conclude that ROCK inhibition blocks accumulation of cortical F-actin and significantly diminishes the capacity for Eph/ephrin-mediated cell sorting in culture.

To assess the role of actin cables in the mammalian embryo, we next examined the facial mesenchyme of E13.5 embryos, a region that exhibits particularly dramatic cell segregation in *Efnb1*$^{Δ/+}$ embryos. Co-staining sections with fluorescently tagged phalloidin and an antibody against ephrin-B1 revealed increases in F-actin at signaling interface boundaries between ephrin-B1–positive and ephrin-B1–negative domains in *Efnb1*$^{Δ/+}$ embryos (Fig. 6, bottom row) that were absent in WT (*Efnb1*$^{lox/+}$) embryos (Fig. 6, top row). These actin cables were located opposite to the ephrin-B1–expressing region (in ephrin-B1–negative cells in contact with ephrin-B1–positive cells), consistent with the idea that they were induced by ephrin-B1 forward signaling across that signaling interface. We therefore conclude that increased cortical actin is also associated with cell segregation in the mammalian embryo.

ROCK is required for segregation in mammalian embryos

Based on our finding that a differential in cortical actomyosin is generated by forward signaling during cell segregation in cell culture in a ROCK-dependent manner, we tested whether signaling through the Rho-family GTPases Rho, Cdc42, and Rac1 is required for Eph/ephrin-mediated cell segregation in mouse embryos. We generated *Efnb1* heterozygous embryos lacking the ability to signal through ROCK, Cdc42, or Rac1 using floxed alleles of Cdc42 (Wu et al., 2006) or Rac1 (Glogauer et
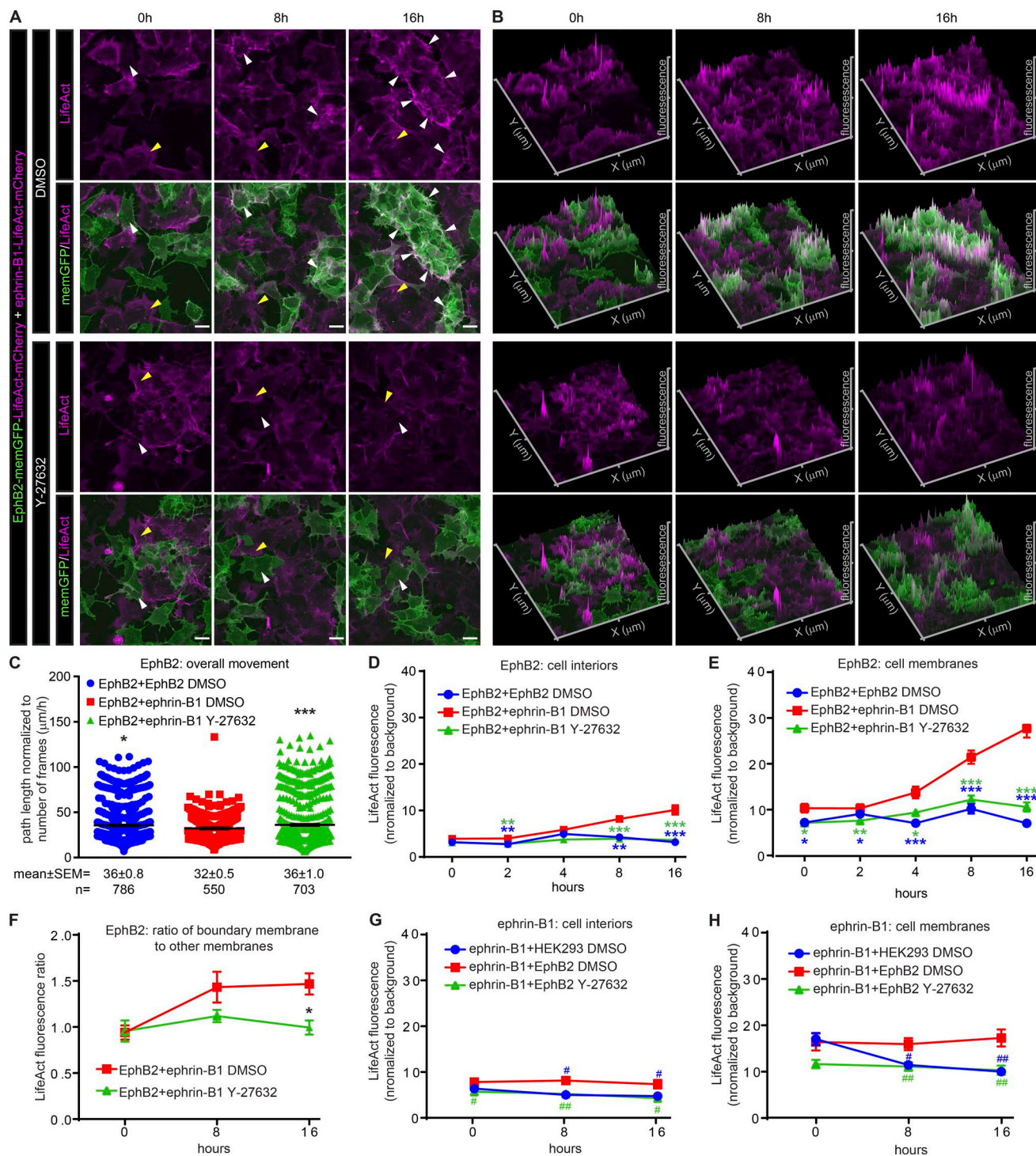
Figure 5.   **Cortical F-actin accumulates in segregating EphB2-expressing cells in a ROCK-dependent manner.** (A) Individual frames from Videos 1 and 2 showing HEK293 cells overexpressing ephrin-B1 and LifeAct-mCherry (magenta; cells marked with yellow arrowheads) mixed with HEK293 cells overexpressing EphB2, membrane-GFP (green), and LifeAct-mCherry (magenta; cells marked with white arrowheads) in the absence (top) or presence (bottom) of Y-27632. Bars, 20 μm. Note the strong increase in cortical F-actin in the EphB2 population (white arrowheads) in the control, but not the Y-27632-treated, condition. (B) 2.5D plots derived from the images in A depicting LifeAct fluorescence intensity on the z axis. (C) Cell tracking analysis of overall EphB2 cell movement over 16 h. (D–E and G–H) LifeAct fluorescence intensities of the cell interiors (D and G) and cell membranes (E and H) of the EphB2-expressing (D–E) and ephrin-B1–expressing (G and H) populations. (F) Ratio of the LifeAct fluorescence intensity at the outside of an EphB2-positive cluster of cells to other cell membranes located inside the cluster. *, P < 0.05; **, P < 0.01; ***, P < 0.0001 compared with EphB2+ephrin-B1 DMSO; #, P < 0.01; ##, P < 0.001 compared with ephrin-B1+EphB2 DMSO. Graphs represent means ± SEM. In A and B, the GFP signal was adjusted in a nonlinear fashion to assist discrimination of the EphB2-expressing population. See also Figs. S2–S5 and Videos 1–6.
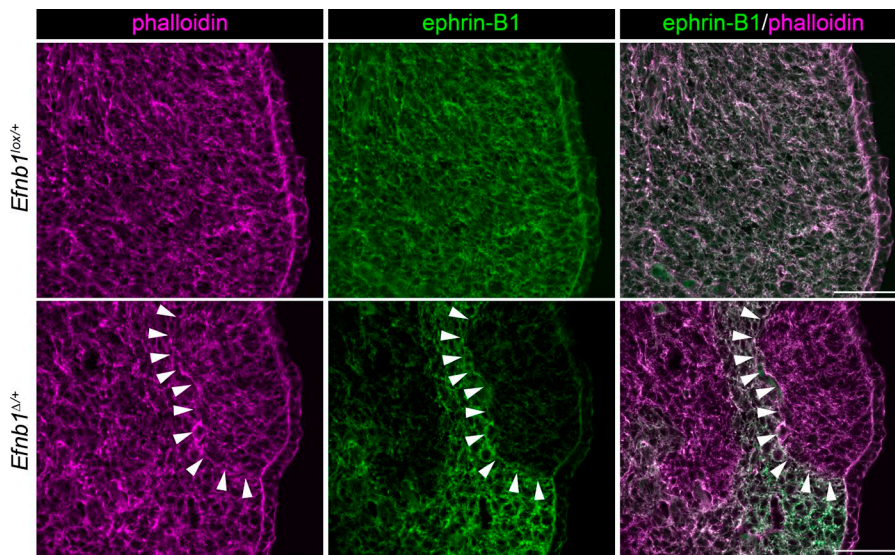
Figure 6. **F-actin cables at ephrin-B1 boundaries in the embryo.** Sections through the palates of control ($Efnb1^{lox/+}$) and heterozygous ($Efnb1^{\Delta/+}$) embryos stained for ephrin-B1 (green) and F-actin (phalloidin; magenta). An ephrin-B1 expression boundary is indicated by white arrowheads. Numbers of embryos analyzed are presented in Table S2. Bars, 50 µm.

al., 2003) or a transgenic conditional dominant-negative allele that interferes with the function of both ROCK1 and ROCK2 (*ROCKDN*; Kobayashi et al., 2004). Because complete loss of function of these signaling mediators results in early embryonic lethality (Sugihara et al., 1998; Chen et al., 2000), we used *Wnt1Cre2* to induce recombination in the neuroepithelium just before neural crest cell emigration and assayed cell segregation in the neural crest cell–derived craniofacial mesenchyme. $Wnt1Cre2^{Tg/+};ROCKDN^{lox/+}$, $Wnt1Cre2^{Tg/+};Cdc42^{lox/lox}$ and $Wnt1Cre2^{Tg/+};Rac1^{lox/lox}$ embryos survive until E11.5 with phenotypes resembling those previously reported (Thomas et al., 2010; Phillips et al., 2012; Liu et al., 2013; unpublished data). Whereas $Wnt1Cre2^{Tg/+};Efnb1^{loxXGFP/+}$ embryos exhibited robust cell segregation in neural crest–derived tissues by E11.5, in $Wnt1Cre2^{Tg/+};Efnb1^{loxXGFP/+};ROCKDN^{lox/+}$ embryos, we observed significantly decreased sorting throughout the neural crest–derived tissues (Fig. 7 A). Quantifying sorting in the lateral nasal process (LNP) revealed that expression of dominant negative ROCK increased the proportion of GFP+ cells in small patches and decreased the proportion of GFP+ cells in large patches (Fig. 7 B), resulting in an overall decrease in the size of the sorted patches (Fig. 7 C). Surprisingly, despite previous in vitro studies supporting roles for Cdc42 and Rac1 in Eph/ephrin signaling, deletion of Cdc42 or Rac1 did not impair cell segregation (Fig. 7, D–I). These data indicate that ROCK activity is also necessary for ephrin-B1–mediated cell segregation in the embryo.

Discussion

Whereas previous studies suggested that bidirectional signaling mediates cell sorting (Durbin et al., 1998; Xu et al., 1999; Mellitzer et al., 2000; Barrios et al., 2003), our data show that reverse signaling through ephrin-B1 by known mechanisms is not required for segregation in the mammalian neuroepithelium. Consistent with this mechanism, during cell segregation in HEK293 cells, EphB2-expressing cells exhibited ROCK-dependent increases in cortical actin, whereas ephrin-B1–expressing cells did not. These results lead us to propose a new model for Eph/ephrin-mediated cell segregation in the mammalian embryo (Fig. 8). Unidirectional, kinase-dependent forward signaling results in elevation of cortical actomyosin specifically within the EphB receptor cell population, creating a differential between the ephrin-B1 and EphB2 cell populations. The unidirectional regulation of cortical actin may contribute to cell segregation by multiple mechanisms.

First, cellular repulsion and migration, mediated by actomyosin contractility in response to ephrin-B1 forward signaling, could lead to grouping of EphB2-expressing cells. If unidirectional repulsive cellular migration drives cell segregation, however, we would expect that EphB2 cells would travel a greater distance, as they are repeatedly redirected over the course of their segregation. Because we observe a decrease in total cell migration of EphB2 cells when undergoing cell segregation (Fig. 5 C), we do not think that repulsive migration is the only driver of cell segregation.

Second, unidirectional signaling might set up a cell adhesion differential. Previous studies in cell culture have indicated that activation of forward signaling can lead to recruitment of ADAM metalloproteases and cleavage of E-cadherin at Eph/ephrin signaling interfaces, which may be particularly relevant in the intestinal epithelium (Solanas et al., 2011). Though our HEK293 cell experiments do not support a requirement of ADAM metalloprotease activity in this system, it remains possible that unidirectional signaling could regulate the expression or localization of adhesion molecules in the forward-signaling recipient cells. This mechanism could also involve signaling through ROCK. For example, in *Xenopus laevis*, actomyosin contractility is critical to reduce cadherin adhesion at the boundary between the notochord and paraxial mesoderm (Fagotto et al., 2013).

Third, it has been more recently shown that cell segregation can occur by differences in cortical tension between cells, leading to a change in the force of the cell–cell contact, or interfacial tension. The actomyosin cytoskeleton is thought to be critical for interfacial tension-driven segregation, with prominent F-actin cables often forming at heterotypic boundaries, and cells with differences in ROCK activity segregate in vitro (Krieg et al., 2008; Monier et al., 2010). Therefore, our observation of elevated cortical actin in EphB2-expressing cells before the formation of larger EphB2 groups leads us to propose that this up-regulation may lead to a change in cortical tension that directly contributes to cell segregation by changing differential
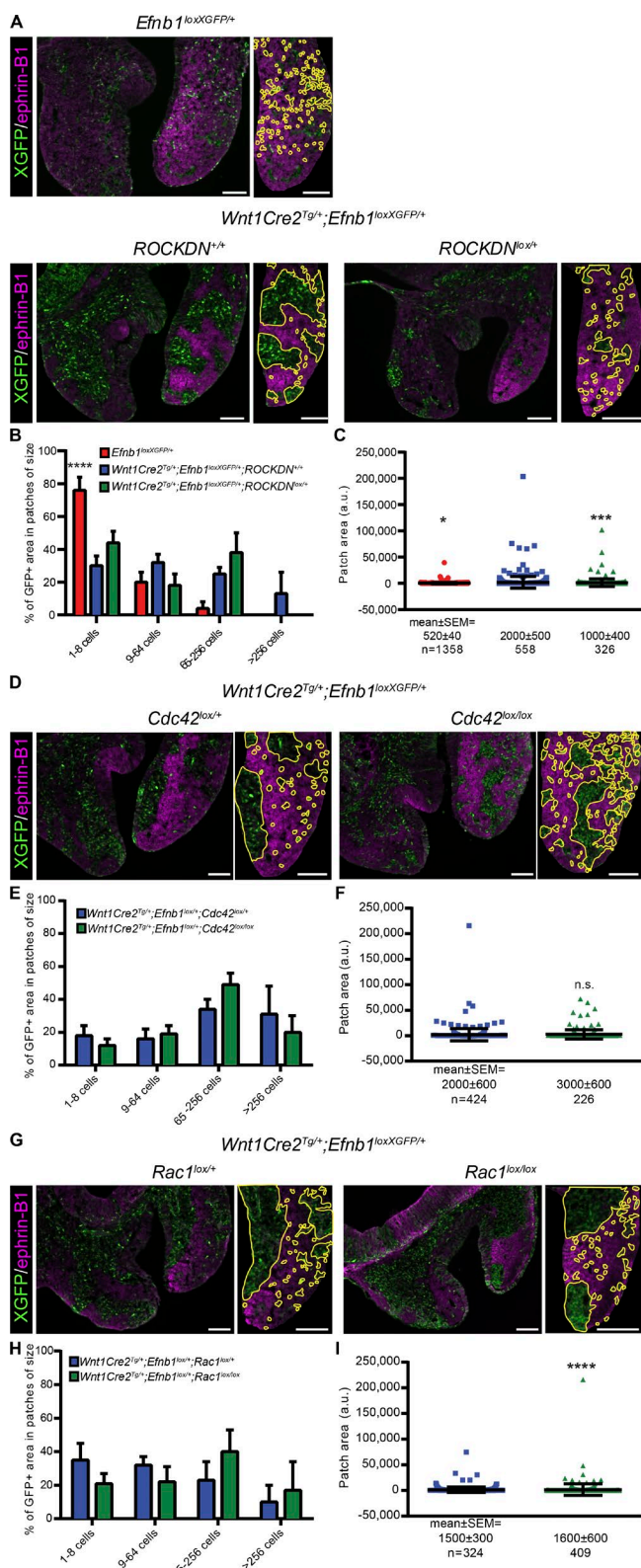
interfacial tension (Fig. 8). In an intermingled population of EphB- and ephrin-B–expressing cells, unidirectional activation of signaling results in populations with differences in cortical actomyosin contractility. Cell segregation in this system occurs as EphB2 cells increase their cortical actin accumulation to levels higher than those observed in ephrin-B1 cells (Fig. 5, compare D and E to G and H). Notably, cortical actin increases most dramatically at the membrane of EphB2 cells in contact with ephrin-B1 cells relative to the homotypic EphB2–EphB2 interfaces (Fig. 5 F). These cell behaviors and changes in cortical actin fit well with the predictions of the DITH, which states that two populations of cells with a differential in interfacial tension (i.e., the force of the contact between two cells) will sort out based on the differences in this tension (Brodland, 2002).

After the initial segregation of EphB2-expressing cells, boundaries were sharpened by the formation of actomyosin cables, thereby excluding ephrin-B1–expressing cells. This observation is consistent with a recent study showing that after the establishment of a boundary by repeated rounds of adhesion and repulsion, accumulation of F-actin occurred at the boundary between the mesoderm and blastocoel roof in *Xenopus* (Rohani et al., 2011). Likewise, in *Xenopus*, myosin contractility is critical to reduce cadherin adhesion at the boundary between the notochord and paraxial mesoderm (Fagotto et al., 2013). Similarly, knockdown of EphA4 in the zebrafish hindbrain resulted in loss of actomyosin cables and a less straight rhombomere boundary (Calzolari et al., 2014). Cortical actomyosin also maintains sharp tissue boundaries in *Drosophila* (Landsberg et al., 2009; Monier et al., 2010), and recently, it has been shown that the Eph receptor shapes the anteroposterior compartment boundary in the *Drosophila* wing disc, though whether this is achieved by regulation of cortical actomyosin contractility has not yet been examined (Umetsu et al., 2014).

It is notable that cell segregation in the embryo depends on ROCK, but not Cdc42 or Rac1, activity. Our genetic studies show that ROCK activity is required for Eph/ephrin-mediated cell segregation in the mouse embryo, and live-cell imaging studies indicate that ROCK activity is required for establishment of a cortical actin differential during segregation. Rho/ROCK has been shown to be required for Eph/ephrin-dependent changes in cell contractility and cytoskeletal collapse (Noren and Pasquale, 2004; Nievergall et al., 2012), and signaling through RhoA/ROCK is required for cell segregation in *Xenopus* animal cap

Figure 7. Signaling through ROCK is required for ephrin-B1–mediated cell segregation in mouse embryos. (A, D, and G) Comparison of patches resulting from aberrant cell segregation in the frontonasal processes of E11.5 *Wnt1Cre2^Tg/+;Efnb1^loxXGFP/+* embryos. Sections were stained for ephrin-B1 (magenta) and GFP (green), and GFP-positive cells and patches in the lateral nasal process (cropped images) were quantified and are outlined in yellow for clarity. Bars, 100 µm. (A) An unsorted embryo (*Efnb1^loxXGFP/+*) compared with an *Efnb1* heterozygous embryo (*Wnt1Cre2^Tg/+;* *Efnb1^loxXGFP/+;ROCKDN^+/+*) and an *Efnb1* heterozygous embryo with Wnt-1Cre2-induced expression of dominant-negative ROCK (*Wnt1Cre2^Tg/+;Efnb1^loxXGFP/+;ROCKDN^lox/+*). (D) Control heterozygous embryo (*Wnt1Cre2^Tg/+;Efnb1^loxXGFP/+;Cdc42^lox/+*) compared with a heterozygous embryo with loss of Cdc42 (*Wnt1Cre2^Tg/+;Efnb1^loxXGFP/+;Cdc42^lox/lox*). (G) Control heterozygous embryo (*Wnt1Cre2^Tg/+;Efnb1^loxXGFP/+;Rac1^lox/+*) compared with a heterozygous embryo with loss of Rac1 (*Wnt1Cre2^Tg/+;Efnb1^loxXGFP/+;Rac1^lox/lox*). (B, E, and H) Distribution of GFP-positive areas into patches of various sizes. Column heights represent means of the distributions in each embryo, and error bars represent SEM. ****, P < 0.0001 as compared with *Wnt1Cre2^Tg/+;Efnb1^loxXGFP/+*. (C, F, and I) Patch sizes represented as scatterplots. Horizontal bars represent means, and error bars represent SEM. *, P < 0.05; ***, P < 0.001, compared with *Wnt1Cre2^Tg/+;Efnb1^loxXGFP/+*; ****, P < 0.0001 compared with *Wnt1Cre2^Tg/+;Efnb1^loxXGFP/+;Rac1^lox/+* control group. Red symbols, *Efnb1^loxXGFP/+*. Blue symbols, *Wnt1Cre2^Tg/+;Efnb1^loxXGFP/+;ROCKDN^+/+, Wnt1Cre2^Tg/+;Efnb1^loxXGFP/+;Rac1^lox/+,* or *Wnt1Cre2^Tg/+;Efnb1^loxXGFP/+;Cdc42^lox/+*. Green symbols, *Wnt1Cre2^Tg/+;Efnb1^loxXGFP/+;ROCKDN^lox/+,* *Wnt1Cre2^Tg/+;Efnb1^loxXGFP/+;* *Rac1^lox/lox,* or *Wnt1Cre2^Tg/+;Efnb1^loxXGFP/+;Cdc42^lox/lox*. Number of embryos analyzed are presented in Table S2.
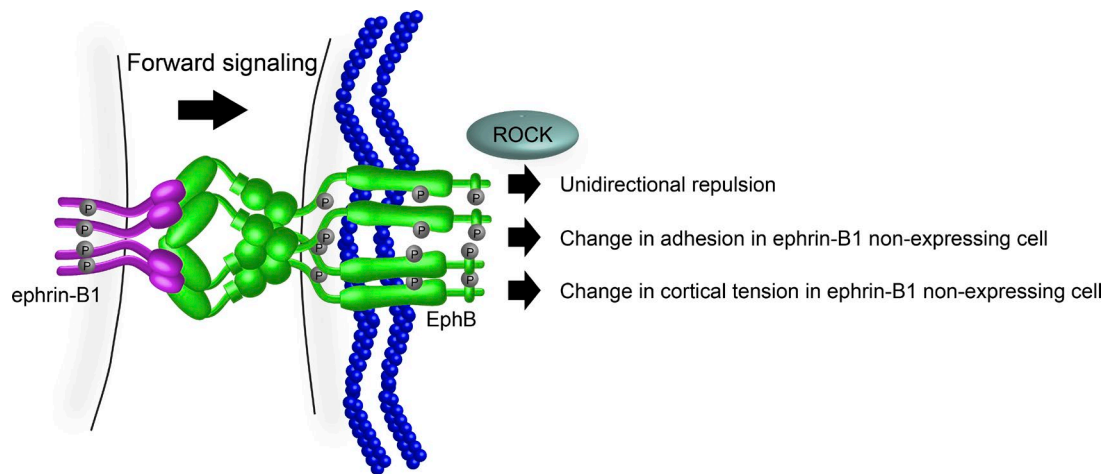
Figure 8. Models of ephrin-B1–driven cell segregation. Based on our work in the mouse embryo, we conclude that unidirectional forward signaling drives cell segregation. Possible mechanisms for unidirectional signaling in cell segregation include unidirectional regulation of repulsive migration and unidirectional regulation of cell adhesion. Based on our live imaging data, we propose a third mechanism, whereby unidirectional signaling leads to a differential in cortical actin between signaling and receiving cells. We suggest that this differential drives segregation by a mechanism that fits the differential interfacial tension hypothesis.

cells, although in this case, bidirectional signaling was proposed to be involved, and the cellular behaviors driving segregation were not clear (Tanaka et al., 2003). A previous study noted multiple, though sometimes contradictory, changes in the activity of Rac1 and Cdc42 upon Eph/ephrin signaling activation (Nievergall et al., 2012). Our data suggest that Rac1 and Cdc42 activity are individually dispensable for Eph/ephrin-mediated cell segregation in the mammalian embryo, though compensation cannot be ruled out. These findings have interesting similarities with ephrin-B2–induced cellular retraction in human umbilical endothelial cells, which was found to depend largely on Rho/ROCK, but not Rac1 (Groeger and Nobes, 2007). In this system, Rho/ROCK-mediated actomyosin contractility is required for cell collapse, whereas Rac regulates termination of EphB receptor signaling by endocytosis. Further, cell collapse was completely inhibited by the joint inhibition of Cdc42 and ROCK. Similarly, we find that interfering with ROCK activity dramatically reduced cell segregation but did not completely block it. Although this might be attributable to incomplete inhibition in the Y-27632 and *ROCKDN* experiments, it is also possible that other pathways and/or pathway redundancy are also at play. Together, these similarities may suggest that actomyosin-mediated cellular collapse and cell segregation are directly related cellular processes. Interestingly, we observed that the PI3K inhibitor GDC0941 increased segregation in cell culture, implying that signals downstream of PI3K/Akt may oppose cell segregation. We speculate that this may be related to PI3K's known roles in promoting Eph/ephrin-regulated cell migration (Genander et al., 2009), which we find is decreased during ephrin-B1–mediated cell segregation (Fig. 5 C). Perhaps by dampening overall migration, the PI3K inhibitor allows segregation mediated by differential cortical tension to proceed more efficiently; however, more investigation of this phenomenon is required.

Notably, the data presented here may further explain the pathogenesis of CFNS and suggest possible treatment approaches. For example, the kinase dependence of cell segregation suggests that specific inhibitors of ephrin-B1/EphB2 signaling might be useful for inhibiting pathogenic cell sorting and could be used as a rational medical treatment approach for CFNS, especially as prenatal genetic diagnostics continue to improve. Whether and how cell segregation ultimately exerts its effects on dysmorphogenesis is an ongoing area of investigation, but this process may include changes in cell proliferation rate across boundaries established by cell segregation (Bush and Soriano, 2010). Thus, the data presented here may shed light on CFNS pathogenesis as well as the fundamental mechanisms used by Eph/ephrin signaling in tissue organization during development and disease.

Materials and methods

Mouse breeding and alleles

All animal experiments were performed in accordance with the protocols of the University of California, San Francisco Institutional Animal Care and Use Committee. Mice were housed under a 12-h light/dark cycle with food and water ad libitum. Mice were socially housed (n = 2–5 per cage) except when single housing was required for breeding or drug-delivery purposes, in which case additional enrichment was provided. For a full description of all genetic crosses used in this paper, see Table S1. *Efnb1^{lox}*, *Efnb1^{6FΔV}*, *X^{GFP}*, *Ephb2^{LacZ}*, *Ephb3^−*, *Ephb1^{AS-KI}*, *Ephb2^{AS-KI}*, *Ephb3^{AS-KI}*, *Cdc42^{lox}*, *Rac1^{lox}*, and *ROCKDN^{lox}* alleles have been previously described (Henkemeyer et al., 1996; Orioli et al., 1996; Hadjantonakis et al., 1998; Glogauer et al., 2003; Davy et al., 2004; Kobayashi et al., 2004; Wu et al., 2006; Bush and Soriano, 2009; Soskis et al., 2012). *ROCKDN^{lox}* mice were provided by the RIKEN BioResource Center through the National Bio-Resource Project of the Ministry of Education, Culture, Sports, Science and Technology, Japan. Recombination of floxed alleles was accomplished by expressing *β-actin-Cre* (MGI: 2176050; resulting in the *Efnb1^Δ* allele) or *Wnt1Cre2* (MGI: 5485027; Lewis et al., 2013). Mouse strain information, the crosses used to generate embryos, and the numbers of embryos are detailed in Table S2. To achieve X chromosome mosaicism, all embryos were female and were collected at E7.5–E13.5 as indicated in the figures.

Histology, immunofluorescence, and quantification of patch areas in embryos

Embryos were processed, sectioned, and subjected to immunofluorescence analysis as described previously (Lewis et al., 2013). For sections

in Fig. 7, images were acquired on an Axio Imager.Z2 upright micro-scope (ZEISS) at room temperature using Cy2 and Cy3 fluorochromes, a 10× air Plan-ECPlan-NeoFluar objective lens (numerical aperture 0.3; ZEISS) and an AxioCamMR3 camera (ZEISS); Axiovision Rel. 4.8 software was used to acquire images, adjust brightness and contrast, and export tiff images. For sections in Fig. 6, single optical sections were acquired on an Axio Observer.Z1 spinning disk confocal micro-scope (ZEISS) at room temperature using Cy2 and Alexa Fluor 647 fluorochromes, a 40× water LD C-Apochromat objective lens (numerical aperture 1.1; ZEISS), and an Axiocam 506 camera (ZEISS). For whole E7.75–E8.5 embryos, confocal stacks were acquired using the same setup but with a 10× air Plan-Apochromat objective lens (numerical aperture 0.45; ZEISS) or, for Fig. 1, on a TI inverted microscope stand (Nikon) equipped with a Borealis-modified Yokogawa CSU-X1 confocal head (Spectral Applied Research) at room temperature using Cy2 and Cy3 fluorochromes, a 10× air Plan Apo objective lens (numerical aperture 0.45; Nikon), a Clara cooled scientific grade interline CCD camera (Andor Technology), and NIS-Elements software. Zen software or ImageJ was used to make maximum projections, adjust brightness and contrast, and export tiff images. For quantification of sorting in *Wnt1Cre2^{Tg/+};Efnb1^{loxXGFP/+}* embryos bearing mutations in Cdc42, Rac1, or ROCK, patch sizes were analyzed in two sections from each of three (for Cdc42), four (for Rac1), or five (for ROCK) embryos for each genotype. Sections from experimental and control embryos were selected and matched based on anatomy. Based on the merged images, each LNP was defined by the dorsal edge of the nasal pit and selected using ImageJ. The LNP was chosen for quantification based on its relatively defined anatomy. Each GFP-positive cell or patch of cells in the LNP was outlined by a blinded observer and quantified using CellProfiler2.1.1 (Carpenter et al., 2006; Lamprecht et al., 2007). For statistical analysis of the distribution of GFP-positive areas, two-way analysis of variance (ANOVA; followed by Dunnett's tests, if necessary) was used. For statistical analysis of patch sizes, Kruskal–Wallis tests (with Dunn's post hoc tests) or Mann–Whitney tests were used.

1-NA-PP1 delivery

Pregnant dams were treated with 80 mg/kg 1-NA-PP1 (dissolved at 3 mg/ml in 10% DMSO/20% Cremaphor/70% PBS; Tocris Bioscience) or a similar amount of vehicle administered by subcutaneous injection of 0.5–0.8 ml drug solution (depending on mouse weight) between the scapulae. Pregnant dams were injected every 8 h starting at E7.5 and were sacrificed for analysis at E8.5.

Quantitative RT-PCR for *Efnb1*, *Ephb2*, and *Ephb3* expression

RNA was isolated from pools of two or three embryos using an RNEasy Mini kit (QIAGEN), and each pool was treated as a single sample. Reverse transcription was performed using a Superscript II RT kit (Invitrogen), and quantitative PCR was performed using iTaq Universal SYBR Green and a CFX96 Real Time System (both from Bio-Rad) and the following primers: efnb1 forward, 5′-CGTTGGCCAAGAACCTGG AGC-3′; efnb1 reverse, 5′-TCCAGCTTGTCTCCAATCTTCGG-3′; ephb2 forward, 5′-TGCTGCTGCCGCTGCTAGC-3′; ephb2 reverse, 5′-TGCTAGCCGCTCACCTCTTTCC-3′; ephb3 forward, 5′-GCTACA CCTTTGAGGTGCAGGC-3′; ephb3 reverse, 5′-GTTGTACGGAGT TCTTCTGGC-3′; GAPDH forward, 5′-ACCACAGTCCATGCCATC AC-3′; GAPDH reverse, 5′-TCCACCACCCTGTTGCTGTA-3′. *Efnb1* and *Ephb* expression levels were normalized to the amount of *GAPDH* and then to mean expression in the E7.75 samples, which was set at 1.0.

HEK293 cell culture, static analysis of sorting, and live-cell imaging

In this system, HEK293 cells expressing GFP and high levels of EphB2 are mixed with either WT HEK293 cells (which express low levels of ephrin-B1) or HEK293 cells expressing high levels of ephrin-B1; the latter condition results in dramatic segregation. Stable HEK293 cell lines expressing ephrin-B1 or EphB2 plus membrane-targeted GFP (EphB2 + GFP) were obtained from A. Poliakov and D. Wilkinson (laboratory of D. Wilkinson, Medical Research Council National Institute for Medical Research, London, England, UK; Poliakov et al., 2008; Jørgensen et al., 2009) and cultured at 37°C with 5% CO$_2$ in DMEM supplemented with 10% bovine calf serum, glutamine, and antibiotics. Cell segregation assays were performed essentially as previously described. In brief, two homogenous populations of cells were aliquoted into and thoroughly resuspended in media containing various inhibitors and plated in 24-well dishes coated with 10 µg/ml fibronectin (Sigma-Aldrich) to obtain a final cell density of 150,000/ml; cells were then grown for 24 h until confluence. Phase and GFP images of living cells were acquired on an Axiovert 200 inverted microscope (ZEISS) at room temperature using a 5× air A-Plan objective lens (numerical aperture 0.12; ZEISS) and an AxioCam MR3 camera (ZEISS); Axiovision Rel. 4.8 software was used to acquire images, adjust brightness and contrast, and export tiff images. For each condition, six GFP images were obtained, background was subtracted, and images were manually thresholded in ImageJ. Images for which manual thresholding was impossible (because of high signal-to-noise ratio in part of the image) were omitted from analysis, resulting in $n = 3–6$ images being included in the final analysis. Segregation was then quantified using a nearest-neighbor method (Mochizuki et al., 1998; Poliakov et al., 2008). In this method, a photograph is converted to a lattice of squares that roughly correspond to cells, each of which is scored as "stained" or "unstained" (in this case, GFP positive or negative). For each square that is stained, the number of neighboring stained squares among the four nearest neighbors (up, down, right, and left) is counted, and this information is used to generate a sorting score as detailed previously (Mochizuki et al., 1998). Sorting scores were normalized to the EphB2-GFP + 293 condition (negative control; set to 0.5) for display purposes, and raw data from three to six images per condition were averaged and analyzed using ANOVA and Dunnett's tests; all conditions were compared with the positive control condition (EphB2 + ephrin-B1 + DMSO). The data in Fig. S4 are representative of three independent experiments for each inhibitor. Of these, Rho inhibitor, Y-27632 and ML7 resulted in decreases in segregation that were close in magnitude to that elicited by unclustered ephrin-B1-Fc, a positive control that blocks ephrin-B1–EphB2 binding (Fig. S4).

For live imaging, HEK293 cells expressing ephrin-B1 or EphB2 and GFP were stably transfected with a LifeAct-mCherry plasmid using Lipofectamine LTX with Plus reagent (15338100; Invitrogen) according to the manufacturer's protocol. Clones were selected based on fluorescence. Equal numbers of EphB2-GFP-LifeAct-mCherry and ephrin-B1-LifeAct-mCherry cells were mixed and plated in a glass-bottomed imaging dish coated with 10 µg/ml fibronectin (Sigma-Aldrich) to a final cell density of 400,000/ml (for most experiments) or 60,000/ ml (for low-density experiments). Mixing was performed in the presence of 20 µM Y-27632 or vehicle (0.2% DMSO). Live imaging was performed at 37°C beginning 1 h after plating; 15 mM Hepes was added and the dish sealed to buffer CO$_2$. Confocal stacks ($3 × 2$ µm) were acquired every 10 min for 16 h using an Axio Observer.Z1 spinning disk confocal microscope (ZEISS) at 37°C, a 40× water LD C-Apochromat objective lens (numerical aperture 1.1; ZEISS), and an Axiocam 506 camera (ZEISS). Zen software was used to acquire images, generate maximum intensity projections (which were then used for display, 2.5D plotting, and image analysis), make 2.5D plots representing LifeAct and GFP intensity, and export avi videos and tiff images. Four videos at high density and six videos at low density were acquired, and cell tracking analysis was performed using the Manual Tracking plugin in

ImageJ. Cells that could not be tracked for at least 12 consecutive frames (2 h in real time) were excluded from the analysis. For linescan analysis, which was performed in ImageJ, seven to ten cells were analyzed per experimental time point per video, for a total of three or four experiments and 27–38 cells per time point (for the high-density experiments) and six experiments and 45–57 cells per time point (for the low-density experiment). In brief, two perpendicular lines (width = 25 pixels, which corresponds to 4 μm) were drawn across each cell, and the values for the membrane and interior LifeAct fluorescence intensities were derived from these linescans. For EphB2 cells in clusters, the first line was drawn perpendicular to the cluster boundary, and the second line was drawn parallel to the cluster boundary, allowing separate analysis of the "boundary" membrane. For statistical analysis, ANOVAs (with Dunnett's post hoc tests) or t tests or Kruskal–Wallis (with Dunn's post hoc tests) or Mann–Whitney tests were used (as detailed in the Statistics section and in the figure legends).

Generation of ROCK1/2 knockout cell lines

HEK293 cells expressing EphB2 and membrane-targeted GFP were subjected to CRISPR/Cas9-mediated mutagenesis of *ROCK1* and *ROCK2* (Ran et al., 2013) using the following sgRNAs: *ROCK1*, 5′-CCGAUUUGGGAUCCCGCAGC-3′ (specificity score from crispr.mit.edu: 91); *ROCK2*, 5′-UCGUCACAAGGCAUCGCAGA-3′ (specificity score: 86). Clones were selected based on PCR amplification and sequencing using the primers: ROCK1 forward, 5′-AAGAGGGCATTGTCACAGCA-3′; ROCK1 reverse, 5′-GCAAACAATCCGAATTCACTTCC-3′; ROCK2 forward, 5′-GGTTGTTAGAAATGTTCTCCTT-3′; ROCK2 reverse, 5′-GCTGTACCTGAACCACCCAGG-3′. For each of the clones used, we did not obtain the WT band of expected size and instead found multiple indels in the *ROCK1* and *ROCK2* loci. Clone A had a 185-bp insertion in *ROCK1* and a 107-bp deletion in *ROCK2*. Clone B had a 131-bp insertion in *ROCK1* and two distinct deletions in the *ROCK2* alleles (one of 13 bp and one of 55 bp). All of these indels are predicted to cause frameshifts, and Western blotting confirmed the loss of ROCK1 and ROCK2 protein (Fig. S5 B). Clones A and B were sequenced for the top three predicted off-target sequences for each sgRNA, and all off targets matched the reference sequences, indicating that these sgRNAs were specific for their targets. These cells were mixed with ephrin-B1/LifeAct-mCherry cells as described in the HEK293 cell culture, static analysis of sorting, and live-cell imaging section and were fixed, permeabilized and stained with Alexa Fluor 647–conjugated phalloidin (1:100; A22287; Thermo Fisher Scientific) before being photographed and subjected to linescan analysis of phalloidin staining as described in the HEK293 cell culture, static analysis of sorting, and live-cell imaging section.

Immunoblotting

Cells were lysed in NP-40 lysis buffer (20 mM Tris-HCl, 137 mM NaCl, 10% glycerol, 1% NP-40, and 2 mM EDTA) supplemented with 1 mM dithiothreitol (Sigma-Aldrich) and the following protease and phosphatase inhibitors: 2 μg/ml aprotinin, 5 μg/ml leupeptin, 1 μg/ml pepstatin, 1 mM PMSF, 10 mM NaF, and 1 mM $NaVO_4$. The amount of protein in each sample was quantified using a BCA Assay (Thermo Fisher Scientific). Immunoblotting was performed according to standard procedures using 10% tris-glycine-polyacrylamide gels (Bio-Rad Laboratories) and Odyssey TBS blocking buffer (LI-COR Biosciences). Imaging of immunoblots was performed using an Odyssey Infrared Imaging System (LI-COR Biosciences), and analysis was performed using Image Studio software (LI-COR Biosciences).

Antibodies

Mouse embryos were subjected to immunofluorescence using 2 μg/ml ephrin-B1 (AF473; R&D Systems), 2 μg/ml EphB2 (AF467; R&D Systems), 2 μg/ml EphB3 (AF432; R&D Systems), and 10 μg/ml GFP (ab13970; Abcam) antibodies. The following secondary antibodies were used: Alexa Fluor 488–conjugated donkey anti–chicken IgG (1:1,000, 703-545-155; Jackson ImmunoResearch Laboratories, Inc.) and Cy3-conjugated donkey anti–goat IgG (1:400; 705-165-003; Jackson ImmunoResearch Laboratories, Inc.). To label F-actin, Alexa Fluor 647–conjugated phalloidin (1:40; A22287; Thermo Fisher Scientific) was used. For Western blotting, the following primary antibodies were used: rabbit anti-ROCK1 (1:500; sc-5560; Santa Cruz Biotechnology, Inc.), ROCK2 (1:500; sc-5561; Santa Cruz Biotechnology, Inc.), and HSP70 (1:1,000; 610607; BD). The following IRDye secondary antibodies were used: goat anti–mouse 680RD (1:5,000; 925–68070; LI-COR Biosciences) and goat anti–rabbit 800CW (1:5,000; 926–32211; LI-COR Biosciences).

Inhibitors used in cell segregation screen

Inhibitors used in cell segregation screen were 2 μg/ml unclustered ephrin-B1-Fc (R&D Systems), 20 μM UO126 (LC Labs), 1 μM PF573228 (Sigma-Aldrich), 1 μM GDC0941 (Genentech), 5 μM IPA3 (Sigma-Aldrich), 10 μM TAPI-1 (EMD Millipore), 10 μM NSC23766 (Santa Cruz Biotechnology, Inc.), 10 μM ML141 (EMD Millipore), 2 μg/ml Rho inhibitor (cell-permeable C3 transferase; Cytoskeleton, Inc.), 20 μM Y-27632 (Cayman), and 25 μM ML7 (EMD Millipore).

Statistics

All statistical tests were performed in GraphPad Prism 6. Assumptions of normality and equal variance were tested using D'Agostino-Pearson omnibus and Bartlett's tests, respectively. Where the sample size was too small to allow for such tests, or where these assumptions were met, ANOVA analysis (with Dunnett's tests) or t tests were performed. Where these assumptions were not met, Kruskal–Wallis tests (with Dunn's tests) or Mann–Whitney tests were used. Where distributions were unequal, log-transforming the data resulted in normal data with equal variances; in this case, ANOVAs (with Dunnett's tests) or t tests were performed on the log-transformed data.

Online supplemental material

Table S1 lists mouse genetic crosses used to generate embryos for experiments in this paper. Table S2 lists the number of embryos examined to generate data for each figure. Videos 1–4 show cortical F-actin accumulation by LifeAct-mCherry fluorescence in EphB2-expressing cells during cell segregation, but not upon inhibition of ROCK with Y-27632 or in controls in which ephrin-B1 or EphB2 cells are not undergoing segregation. Videos 5 and 6 show increases in LifeAct-mCherry fluorescence in similar experiments performed at low cell density, and Fig. S3 shows still frames and quantification from these experiments. Fig. S1 shows expression of ephrin-B1, EphB2, and EphB3 in early (approximately E8.5) embryos. Fig. S2 shows that cortical actin does not accumulate in control cells not undergoing segregation. Fig. S4 shows the results of a pharmacologic screen of candidate pathways downstream of Eph/ephrin signaling in HEK293 cell segregation. Fig. S5 shows that ablation of ROCK1 and 2 in EphB2-expressing cells decreases cortical actin accumulation.

References

Barrios, A., R.J. Poole, L. Durbin, C. Brennan, N. Holder, and S.W. Wilson. 2003. Eph/Ephrin signaling regulates the mesenchymal-to-epithelial transition of the paraxial mesoderm during somite morphogenesis. *Curr. Biol.* 13:1571–1582. http://dx.doi.org/10.1016/j.cub.2003.08.030

Batlle, E., and D.G. Wilkinson. 2012. Molecular mechanisms of cell segregation and boundary formation in development and tumorigenesis. *Cold Spring Harb. Perspect. Biol.* 4:a008227. http://dx.doi.org/10.1101/cshperspect.a008227

Birgbauer, E., C.A. Cowan, D.W. Sretavan, and M. Henkemeyer. 2000. Kinase independent function of EphB receptors in retinal axon pathfinding to the optic disc from dorsal but not ventral retina. *Development.* 127:1231–1241.

Brodland, G.W. 2002. The Differential Interfacial Tension Hypothesis (DITH): a comprehensive theory for the self-rearrangement of embryonic cells and tissues. *J. Biomech. Eng.* 124:188–197. http://dx.doi.org/10.1115/1.1449491

Bush, J.O., and P. Soriano. 2009. Ephrin-B1 regulates axon guidance by reverse signaling through a PDZ-dependent mechanism. *Genes Dev.* 23:1586–1599. http://dx.doi.org/10.1101/gad.1807209

Bush, J.O., and P. Soriano. 2010. Ephrin-B1 forward signaling regulates craniofacial morphogenesis by controlling cell proliferation across Eph-ephrin boundaries. *Genes Dev.* 24:2068–2080. http://dx.doi.org/10.1101/gad.1963210

Calzolari, S., J. Terriente, and C. Pujades. 2014. Cell segregation in the vertebrate hindbrain relies on actomyosin cables located at the interhombomeric boundaries. *EMBO J.* 33:686–701. http://dx.doi.org/10.1002/embj.201386003

Carpenter, A.E., T.R. Jones, M.R. Lamprecht, C. Clarke, I.H. Kang, O. Friman, D.A. Guertin, J.H. Chang, R.A. Lindquist, J. Moffat, et al. 2006. CellProfiler: image analysis software for identifying and quantifying cell phenotypes. *Genome Biol.* 7:R100. http://dx.doi.org/10.1186/gb-2006-7-10-r100

Cavodeassi, F., K. Ivanovitch, and S.W. Wilson. 2013. Eph/Ephrin signalling maintains eye field segregation from adjacent neural plate territories during forebrain morphogenesis. *Development.* 140:4193–4202. http://dx.doi.org/10.1242/dev.097048

Cayuso, J., Q. Xu, and D.G. Wilkinson. 2015. Mechanisms of boundary formation by Eph receptor and ephrin signaling. *Dev. Biol.* 401:122–131. http://dx.doi.org/10.1016/j.ydbio.2014.11.013

Chen, F., L. Ma, M.C. Parrini, X. Mao, M. Lopez, C. Wu, P.W. Marks, L. Davidson, D.J. Kwiatkowski, T. Kirchhausen, et al. 2000. Cdc42 is required for PIP(2)-induced actin polymerization and early development but not for cell viability. *Curr. Biol.* 10:758–765. http://dx.doi.org/10.1016/S0960-9822(00)00571-6

Choe, C.P., and J.G. Crump. 2015. Eph-Pak2a signaling regulates branching of the pharyngeal endoderm by inhibiting late-stage epithelial dynamics. *Development.* 142:1089–1094. http://dx.doi.org/10.1242/dev.115774

Compagni, A., M. Logan, R. Klein, and R.H. Adams. 2003. Control of skeletal patterning by ephrinB1-EphB interactions. *Dev. Cell.* 5:217–230. http://dx.doi.org/10.1016/S1534-5807(03)00198-9

Davy, A., J. Aubin, and P. Soriano. 2004. Ephrin-B1 forward and reverse signaling are required during mouse development. *Genes Dev.* 18:572–583. http://dx.doi.org/10.1101/gad.1171704

Davy, A., J.O. Bush, and P. Soriano. 2006. Inhibition of gap junction communication at ectopic Eph/ephrin boundaries underlies craniofrontonasal syndrome. *PLoS Biol.* 4:e315. http://dx.doi.org/10.1371/journal.pbio.0040315

Dravis, C., and M. Henkemeyer. 2011. Ephrin-B reverse signaling controls septation events at the embryonic midline through separate tyrosine phosphorylation-independent signaling avenues. *Dev. Biol.* 355:138–151. http://dx.doi.org/10.1016/j.ydbio.2011.04.020

Durbin, L., C. Brennan, K. Shiomi, J. Cooke, A. Barrios, S. Shanmugalingam, B. Guthrie, R. Lindberg, and N. Holder. 1998. Eph signaling is required for segmentation and differentiation of the somites. *Genes Dev.* 12:3096–3109. http://dx.doi.org/10.1101/gad.12.19.3096

Fagotto, F. 2014. The cellular basis of tissue separation. *Development.* 141:3303–3318. http://dx.doi.org/10.1242/dev.090332

Fagotto, F., N. Rohani, A.-S. Touret, and R. Li. 2013. A molecular base for cell sorting at embryonic boundaries: contact inhibition of cadherin adhesion by ephrin/Eph-dependent contractility. *Dev. Cell.* 27:72–87. http://dx.doi.org/10.1016/j.devcel.2013.09.004

Fagotto, F., R. Winklbauer, and N. Rohani. 2014. Ephrin-Eph signaling in embryonic tissue separation. *Cell Adhes. Migr.* 8:308–326. http://dx.doi.org/10.4161/19336918.2014.970028

Genander, M., M.M. Halford, N.-J. Xu, M. Eriksson, Z. Yu, Z. Qiu, A. Martling, G. Greicius, S. Thakar, T. Catchpole, et al. 2009. Dissociation of EphB2 signaling pathways mediating progenitor cell proliferation and tumor suppression. *Cell.* 139:679–692. http://dx.doi.org/10.1016/j.cell.2009.08.048

Glogauer, M., C.C. Marchal, F. Zhu, A. Worku, B.E. Clausen, I. Foerster, P. Marks, G.P. Downey, M. Dinauer, and D.J. Kwiatkowski. 2003. Rac1 deletion in mouse neutrophils has selective effects on neutrophil functions. *J. Immunol.* 170:5652–5657. http://dx.doi.org/10.4049/jimmunol.170.11.5652

Groeger, G., and C.D. Nobes. 2007. Co-operative Cdc42 and Rho signalling mediates ephrinB-triggered endothelial cell retraction. *Biochem. J.* 404:23–29. http://dx.doi.org/10.1042/BJ20070146

Hadjantonakis, A.-K., M. Gertsenstein, M. Ikawa, M. Okabe, and A. Nagy. 1998. Non-invasive sexing of preimplantation stage mammalian embryos. *Nat. Genet.* 19:220–222. http://dx.doi.org/10.1038/893

Hadjantonakis, A.-K., L.L. Cox, P.P.L. Tam, and A. Nagy. 2001. An X-linked GFP transgene reveals unexpected paternal X-chromosome activity in trophoblastic giant cells of the mouse placenta. *Genesis.* 29:133–140. http://dx.doi.org/10.1002/gene.1016

Henkemeyer, M., D. Orioli, J.T. Henderson, T.M. Saxton, J. Roder, T. Pawson, and R. Klein. 1996. Nuk controls pathfinding of commissural axons in the mammalian central nervous system. *Cell.* 86:35–46. http://dx.doi.org/10.1016/S0092-8674(00)80075-6

Holmberg, J., M. Genander, M.M. Halford, C. Annerén, M. Sondell, M.J. Chumley, R.E. Silvany, M. Henkemeyer, and J. Frisén. 2006. EphB receptors coordinate migration and proliferation in the intestinal stem cell niche. *Cell.* 125:1151–1163. http://dx.doi.org/10.1016/j.cell.2006.04.030

Jørgensen, C., A. Sherman, G.I. Chen, A. Pasculescu, A. Poliakov, M. Hsiung, B. Larsen, D.G. Wilkinson, R. Linding, and T. Pawson. 2009. Cell-specific information processing in segregating populations of Eph receptor ephrin-expressing cells. *Science.* 326:1502–1509. http://dx.doi.org/10.1126/science.1176615

Kobayashi, K., M. Takahashi, N. Matsushita, J. Miyazaki, M. Koike, H. Yaginuma, N. Osumi, K. Kaibuchi, and K. Kobayashi. 2004. Survival of developing motor neurons mediated by Rho GTPase signaling pathway through Rho-kinase. *J. Neurosci.* 24:3480–3488. http://dx.doi.org/10.1523/JNEUROSCI.0295-04.2004

Krieg, M., Y. Arboleda-Estudillo, P.-H. Puech, J. Käfer, F. Graner, D.J. Müller, and C.-P. Heisenberg. 2008. Tensile forces govern germ-layer organization in zebrafish. *Nat. Cell Biol.* 10:429–436. http://dx.doi.org/10.1038/ncb1705

Lamprecht, M.R., D.M. Sabatini, and A.E. Carpenter. 2007. CellProfiler: free, versatile software for automated biological image analysis. *Biotechniques.* 42:71–75. http://dx.doi.org/10.2144/000112257

Landsberg, K.P., R. Farhadifar, J. Ranft, D. Umetsu, T.J. Widmann, T. Bittig, A. Said, F. Jülicher, and C. Dahmann. 2009. Increased cell bond tension governs cell sorting at the *Drosophila* anteroposterior compartment boundary. *Curr. Biol.* 19:1950–1955. http://dx.doi.org/10.1016/j.cub.2009.10.021

Lewis, A.E., H.N. Vasudevan, A.K. O'Neill, P. Soriano, and J.O. Bush. 2013. The widely used Wnt1-Cre transgene causes developmental phenotypes by ectopic activation of Wnt signaling. *Dev. Biol.* 379:229–234. http://dx.doi.org/10.1016/j.ydbio.2013.04.026

Lisabeth, E.M., G. Falivelli, and E.B. Pasquale. 2013. Eph receptor signaling and ephrins. *Cold Spring Harb. Perspect. Biol.* 5:a009159. http://dx.doi.org/10.1101/cshperspect.a009159

Liu, Y., Y. Jin, J. Li, E. Seto, E. Kuo, W. Yu, R.J. Schwartz, M. Blazo, S.L. Zhang, and X. Peng. 2013. Inactivation of Cdc42 in neural crest cells causes craniofacial and cardiovascular morphogenesis defects. *Dev. Biol.* 383:239–252. http://dx.doi.org/10.1016/j.ydbio.2013.09.013

Mellitzer, G., Q. Xu, and D.G. Wilkinson. 2000. Control of cell behaviour by signalling through Eph receptors and ephrins. *Curr. Opin. Neurobiol.* 10:400–408. http://dx.doi.org/10.1016/S0959-4388(00)00095-7

Merrill, A.E., E.G. Bochukova, S.M. Brugger, M. Ishii, D.T. Pilz, S.A. Wall, K.M. Lyons, A.O.M. Wilkie, and R.E. Maxson Jr. 2006. Cell mixing at a neural crest-mesoderm boundary and deficient ephrin-Eph signaling in the pathogenesis of craniosynostosis. *Hum. Mol. Genet.* 15:1319–1328. http://dx.doi.org/10.1093/hmg/ddl052

Mochizuki, A., N. Wada, H. Ide, and Y. Iwasa. 1998. Cell-cell adhesion in limb-formation, estimated from photographs of cell sorting experiments based on a spatial stochastic model. *Dev. Dyn.* 211:204–214. http://dx.doi.org/10.1002/(SICI)1097-0177(199803)211:3<204::AID-AJA2>3.0.CO;2-L

Monier, B., A. Pélissier-Monier, A.H. Brand, and B. Sanson. 2010. An actomyosin-based barrier inhibits cell mixing at compartmental boundaries in Drosophila embryos. *Nat. Cell Biol.* 12:60–65: 1–9. http://dx.doi.org/10.1038/ncb2005

Nievergall, E., M. Lackmann, and P.W. Janes. 2012. Eph-dependent cell-cell adhesion and segregation in development and cancer. *Cell. Mol. Life Sci.* 69:1813–1842. http://dx.doi.org/10.1007/s00018-011-0900-6

Noren, N.K., and E.B. Pasquale. 2004. Eph receptor-ephrin bidirectional signals that target Ras and Rho proteins. *Cell. Signal.* 16:655–666. http://dx.doi.org/10.1016/j.cellsig.2003.10.006

Orioli, D., M. Henkemeyer, G. Lemke, R. Klein, and T. Pawson. 1996. Sek4 and Nuk receptors cooperate in guidance of commissural axons and in palate formation. *EMBO J.* 15:6035–6049.

Phillips, H.M., T. Papoutsi, H. Soenen, P. Ybot-Gonzalez, D.J. Henderson, and B. Chaudhry. 2012. Neural crest cell survival is dependent on Rho kinase and is required for development of the mid face in mouse embryos. *PLoS One.* 7:e37685. http://dx.doi.org/10.1371/journal.pone.0037685

Poliakov, A., M. Cotrina, and D.G. Wilkinson. 2004. Diverse roles of eph receptors and ephrins in the regulation of cell migration and tissue assembly. *Dev. Cell.* 7:465–480. http://dx.doi.org/10.1016/j.devcel.2004.09.006

Poliakov, A., M.L. Cotrina, A. Pasini, and D.G. Wilkinson. 2008. Regulation of EphB2 activation and cell repulsion by feedback control of the MAPK pathway. *J. Cell Biol.* 183:933–947. http://dx.doi.org/10.1083/jcb.200807151

Prospéri, M.-T., P. Lépine, F. Dingli, P. Paul-Gilloteaux, R. Martin, D. Loew, H.-J. Knölker, and E. Coudrier. 2015. Myosin 1b functions as an effector of EphB signaling to control cell repulsion. *J. Cell Biol.* 210:347–361. http://dx.doi.org/10.1083/jcb.201501018

Ran, F.A., P.D. Hsu, J. Wright, V. Agarwala, D.A. Scott, and F. Zhang. 2013. Genome engineering using the CRISPR-Cas9 system. *Nat. Protoc.* 8:2281–2308. http://dx.doi.org/10.1038/nprot.2013.143

Riedl, J., A.H. Crevenna, K. Kessenbrock, J.H. Yu, D. Neukirchen, M. Bista, F. Bradke, D. Jenne, T.A. Holak, Z. Werb, et al. 2008. Lifeact: a versatile marker to visualize F-actin. *Nat. Methods.* 5:605–607. http://dx.doi.org/10.1038/nmeth.1220

Risley, M., D. Garrod, M. Henkemeyer, and W. McLean. 2009. EphB2 and EphB3 forward signalling are required for palate development. *Mech. Dev.* 126:230–239. http://dx.doi.org/10.1016/j.mod.2008.10.009

Rohani, N., L. Canty, O. Luu, F. Fagotto, and R. Winklbauer. 2011. EphrinB/EphB signaling controls embryonic germ layer separation by contact-induced cell detachment. *PLoS Biol.* 9:e1000597. http://dx.doi.org/10.1371/journal.pbio.1000597

Santiago, A., and C.A. Erickson. 2002. Ephrin-B ligands play a dual role in the control of neural crest cell migration. *Development.* 129:3621–3632.

Shi, Y., C.G. Pontrello, K.A. DeFea, L.F. Reichardt, and I.M. Ethell. 2009. Focal adhesion kinase acts downstream of EphB receptors to maintain mature dendritic spines by regulating cofilin activity. *J. Neurosci.* 29:8129–8142. http://dx.doi.org/10.1523/JNEUROSCI.4681-08.2009

Solanas, G., C. Cortina, M. Sevillano, and E. Batlle. 2011. Cleavage of E-cadherin by ADAM10 mediates epithelial cell sorting downstream of EphB signalling. *Nat. Cell Biol.* 13:1100–1107. http://dx.doi.org/10.1038/ncb2298

Soskis, M.J., H.-Y.H. Ho, B.L. Bloodgood, M.A. Robichaux, A.N. Malik, B. Ataman, A.A. Rubin, J. Zieg, C. Zhang, K.M. Shokat, et al. 2012. A chemical genetic approach reveals distinct EphB signaling mechanisms during brain development. *Nat. Neurosci.* 15:1645–1654. http://dx.doi.org/10.1038/nn.3249

Steinberg, M.S. 1963. Reconstruction of tissues by dissociated cells. Some morphogenetic tissue movements and the sorting out of embryonic cells may have a common explanation. *Science.* 141:401–408. http://dx.doi.org/10.1126/science.141.3579.401

Steinberg, M.S. 1970. Does differential adhesion govern self-assembly processes in histogenesis? Equilibrium configurations and the emergence of a hierarchy among populations of embryonic cells. *J. Exp. Zool.* 173:395–433. http://dx.doi.org/10.1002/jez.1401730406

Sugihara, K., N. Nakatsuji, K. Nakamura, K. Nakao, R. Hashimoto, H. Otani, H. Sakagami, H. Kondo, S. Nozawa, A. Aiba, and M. Katsuki. 1998. Rac1 is required for the formation of three germ layers during gastrulation. *Oncogene.* 17:3427–3433. http://dx.doi.org/10.1038/sj.onc.1202595

Tanaka, M., T. Kamo, S. Ota, and H. Sugimura. 2003. Association of Disheveled with Eph tyrosine kinase receptor and ephrin mediates cell repulsion. *EMBO J.* 22:847–858. http://dx.doi.org/10.1093/emboj/cdg088

Taylor, W.R., R. Morley, A. Krasavin, L. Gregory, D.G. Wilkinson, and A. Poliakov. 2012. A mechanical model of cell segregation driven by differential adhesion. *PLoS One.* 7:e43226. http://dx.doi.org/10.1371/journal.pone.0043226

Thomas, P.S., J. Kim, S. Nunez, M. Glogauer, and V. Kaartinen. 2010. Neural crest cell-specific deletion of Rac1 results in defective cell-matrix interactions and severe craniofacial and cardiovascular malformations. *Dev. Biol.* 340:613–625. http://dx.doi.org/10.1016/j.ydbio.2010.02.021

Ting, M.-C., N.L. Wu, P.G. Roybal, J. Sun, L. Liu, Y. Yen, and R.E. Maxson Jr. 2009. EphA4 as an effector of Twist1 in the guidance of osteogenic precursor cells during calvarial bone growth and in craniosynostosis. *Development.* 136:855–864. http://dx.doi.org/10.1242/dev.028605

Twigg, S.R., R. Kan, C. Babbs, E.G. Bochukova, S.P. Robertson, S.A. Wall, G.M. Morriss-Kay, and A.O. Wilkie. 2004. Mutations of ephrin-B1 (EFNB1), a marker for tissue boundary formation, cause craniofrontonasal syndrome. *Proc. Natl. Acad. Sci. USA.* 101:8652–8657. http://dx.doi.org/10.1073/pnas.0402819101

Twigg, S.R.F., C. Babbs, M.E.P. van den Elzen, A. Goriely, S. Taylor, S.J. McGowan, E. Giannoulatou, L. Lonie, J. Ragoussis, E. Sadighi Akha, et al. 2013. Cellular interference in craniofrontonasal syndrome: males mosaic for mutations in the X-linked EFNB1 gene are more severely affected than true hemizygotes. *Hum. Mol. Genet.* 22:1654–1662. http://dx.doi.org/10.1093/hmg/ddt015

Umetsu, D., S. Dunst, and C. Dahmann. 2014. An RNA interference screen for genes required to shape the anteroposterior compartment boundary in Drosophila identifies the Eph receptor. *PLoS One.* 9:e114340. http://dx.doi.org/10.1371/journal.pone.0114340

Wada, N., H. Tanaka, H. Ide, and T. Nohno. 2003. Ephrin-A2 regulates position-specific cell affinity and is involved in cartilage morphogenesis in the chick limb bud. *Dev. Biol.* 264:550–563. http://dx.doi.org/10.1016/j.ydbio.2003.08.019

Wieland, I., S. Jakubiczka, P. Muschke, M. Cohen, H. Thiele, K.L. Gerlach, R.H. Adams, and P. Wieacker. 2004. Mutations of the ephrin-B1 gene cause craniofrontonasal syndrome. *Am. J. Hum. Genet.* 74:1209–1215. http://dx.doi.org/10.1086/421532

Wu, X., F. Quondamatteo, T. Lefever, A. Czuchra, H. Meyer, A. Chrostek, R. Paus, L. Langbein, and C. Brakebusch. 2006. Cdc42 controls progenitor cell differentiation and β-catenin turnover in skin. *Genes Dev.* 20:571–585. http://dx.doi.org/10.1101/gad.361406

Xu, Q., G. Mellitzer, V. Robinson, and D.G. Wilkinson. 1999. In vivo cell sorting in complementary segmental domains mediated by Eph receptors and ephrins. *Nature.* 399:267–271. http://dx.doi.org/10.1038/20452